New type of CFRP reinforcement and technique for the flexural strengthening of RC balconies

Joaquim A.O. Barros [a], Fábio P. Figueiredo [a,*], Inês G. Costa [b], Filipe N.F.M. Dourado [c]

[a] *UMinho - University of Minho, ISISE, Department of Civil Engineering, Guimarães, Portugal*
[b] *CiviTest Lda Company, Jesufrei, Vila Nova Famalicao, Portugal*
[c] *S&P Clever Reinforcement Iberica, Parque Industrial de Argena, Amora, Portugal*

ARTICLE INFO

ABSTRACT

The present work assesses the potentialities of a new carbon fibre reinforced polymer (CFRP) bar, applied according to a hybrid technique for the flexural strengthening of cantilever type reinforced concrete (RC) structures, such as the case of RC balconies. The CFRP bar is formed by an inclined extremity that is inserted into a hole according to the embedded through section (ETS) technique, a part that is applied according to the near-surface mounted (NSM) technique, and a transition zone between these two parts. The anchorage conditions of the ETS part of the CFRP bar allow limiting the strengthening intervention to the cantilever zone of the balcony, with an almost null intrusion to the interior of the building.

The effectiveness of this CFRP reinforcement and technique was assessed by testing 9 double-sided RC balcony prototypes, in a total of 18 tests. The inclination of the ETS part of the CFRP bar (15° and 30°), the concrete strength class (C25 and C35) and the ratio of existing flexural tensile reinforcement (ρ_{ls}=0.28% and 0.44%) were the variables investigated in terms of flexural strengthening performance. The results showed that the strengthening effectiveness has increased with the decrease of the inclination of the ETS part of the CFRP bar. A reinforcement ratio of 0.17% of CFRP bars with an extremity at 15° inclination, has doubled the load-carrying capacity of the corresponding reference prototypes.

The applicability of the most recent formulation of the *fib* bulletin 90 for the flexural strengthening of RC elements with NSM CFRP reinforcements was assessed for this type of application. The ratio between maximum load registered experimentally and predicted with *fib* formulation was 0.95 with a standard deviation of 0.08. However, this high level of predictive performance requires the effective tensile strength of the transition zone of the CFRP bar to be known, which is still a critical aspect of the current generation of CFRP bars. A numerical approach was developed, capable of estimating the force–deflection, the strains and stresses in the constituent materials and evolution of stiffness degradation of the strengthened structures during the loading process, and its high predictive performance was also demonstrated by simulating the experimental tests carried out.

1. Introduction

Experimental research has demonstrated that the flexural strengthening effectiveness provided by CFRP reinforcements applied according to the NSM technique can be conditioned by the occurrence of premature failure modes at the extremity of these reinforcements, currently designated by concrete cover separation or rip-off failure mode [1–3]. In an attempt of avoiding this type of failure model, CFRP wet layup strips of U configuration are usually applied by wrapping the end extremities of the NSM reinforcements, sometimes with the extra functionality of

also providing shear strengthen to the RC beam [4,5]. CFRP wet layup strips of U configuration [6] and CFRP grid U-wraps [7] were also effective in avoiding the occurrence of premature failures modes of CFRP wet layup systems applied for the flexural strengthening of RC beams with the added benefit of increasing their shear capacity. These strengthening strategies have, however, supplementary costs, and their effectiveness is totally lost in case of fire occurrence due to the detrimental susceptibility of externally bonded reinforcements (EBR) to high temperatures [8,9]. Furthermore, it is not applicable in the case of flexural strengthening of RC slabs. FRP reinforcement with a bent
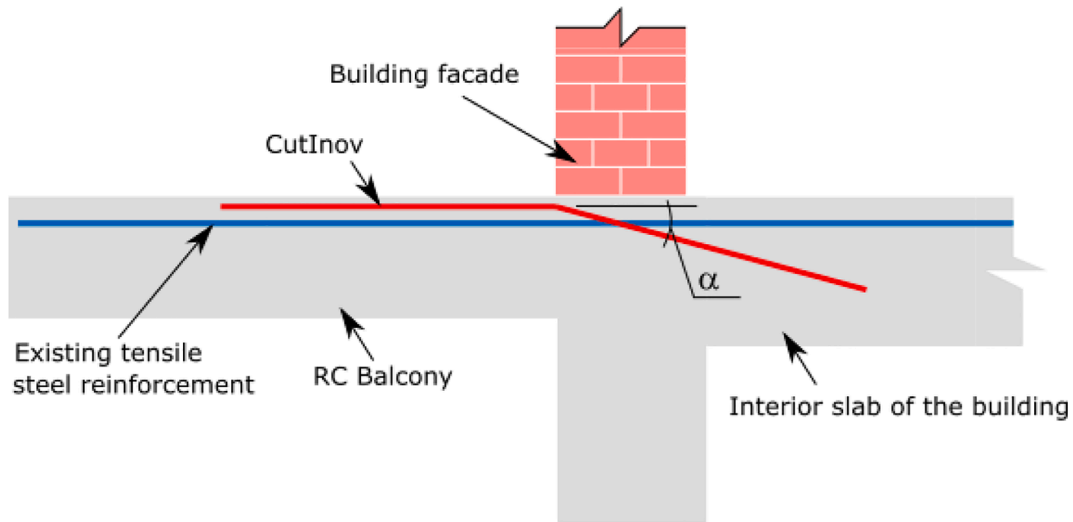
Fig. 1. Flexural strengthening of RC balconies with CutInov CFRP bars.

extremity inserted according to the embedded through section (ETS) technique [10,11] seems to be not susceptible to this detrimental effect, and even in a fire scenario, this FRP can work like a tendon, providing some residual strengthening effect [12]. The extremities of this type of reinforcement, by providing good anchorage conditions to the part of the reinforcement applied according to the NSM technique, will avoid the occurrence of rip-off failure mode, and, depending on the inclination and anchorage length of this part of the reinforcement, applied according to the ETS technique, can contribute for the shear capacity of RC beams [13]. FRP ropes applied according to the NSM and ETS techniques were also used with interesting efficiency in shear strengthening of RC beams [14] and flexural strengthening of support regions of RC beams [15].

Prefabricated pultruded CFRP laminates of rectangular cross-section, thermo-mechanically transformed for having one or two extremities with a certain inclination (clip or sticker type configuration) were firstly used with appreciable efficiency for the simultaneous flexural and punching strengthening of RC slabs [10]. These laminates were formed by one part applied according to the NSM technique, and one or more parts applied according to the ETS technique. The different parts are connected by a transition zone with variable cross-section that reshapes the NSM-CFRP rectangular cross-section to an almost circular one. Pullout tests with this first generation of CFRP reinforcements (designated by the acronym, CutInov) have demonstrated the occurrence of premature failure in the transition zone due to its relatively small tensile strength, in consequence of the thermo-mechanical post-treatment for assuring the aimed inclination of the extremities, and also due to the

multiaxial stress field (axial, bending and shear forces) installed in this curved shape branch of the CFRP reinforcement, as proved by using the developed numerical approach [16].

Recent collapses of RC balconies due to the reduced internal arm and/or corrosion of the tensile reinforcement (top surface), concrete damage or balcony overload, have highlighted the opportunity of using CutInov reinforcements for the flexural strengthening of this type of RC structure with technical and economic advantages. In fact, by executing holes in the support region of the RC balcony, from the external face of the building facade towards the interior, as well as grooves on the concrete cover of the RC balcony, the sticker version of the CutInov bar can be quickly applied without additional intrusion in the building and no alteration of the geometry of the strengthened elements (Fig. 1). Due to the immunity of CFRP to corrosion, this reinforcement applied according to this hybrid NSM-ETS technique is an excellent alternative to the one based on the use of conventional steel reinforcement due to the relatively higher concrete cover thickness this last one requires for its protection from aggressive agents.

The second generation of CutInov CFRP circular cross-section bars is being developed for the flexural strengthening of cantilever type RC elements, such as the RC balconies. The present work assesses, for the first time, the potentialities of these bars by executing an experimental program of 18 tests with prototypes of RC balconies. The effect of the quality of the concrete and the ratio of the existing flexural reinforcement in the performance of this flexural strengthening technique is investigated. Furthermore, the predictive performance of the recent formulation proposed in the *fib* bulletin 90 [17] for estimating the
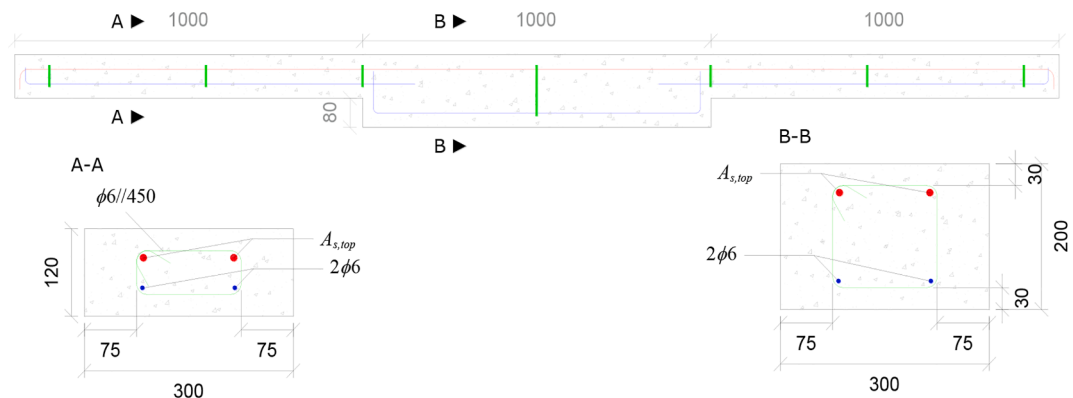

Fig. 2. Schematic representation of the geometry and reinforcements of the prototype for executing two tests of RC balconies (dimensions in mm).
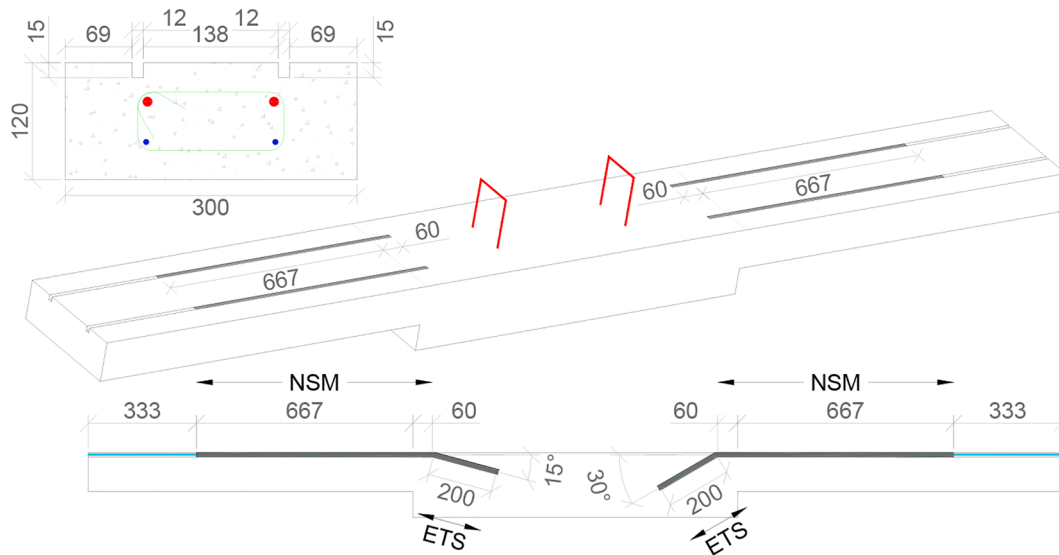
Fig. 3. Strengthening details of the balcony prototypes strengthened with CFRP bars with extremity inclined at 15° and 30° (dimensions in mm).

contribution of NSM-FRP systems for the flexural strengthening of RC elements is assessed. Finally, a comprehensive formulation is proposed for designing flexural strengthening solutions by using CutInov CFRP reinforcements applied according to the NSM-ETS hybrid technique. By simulating the experimentally tested RC balcony prototypes it was demonstrated that the developed approach provides accurate predictions in terms of load-carrying capacity, deflection and stiffness evolution during the loading process.

2. Experimental program

2.1. RC balcony prototypes and series of tests

For assessing the effectiveness of the new type of CFRP bars that are being developed for the flexural strengthening of cantilever type RC structures, such as the case of balconies, the prototype with the geometry and reinforcement details represented in Fig. 2 was adopted. This prototype aims to resemble the loading and supporting conditions of balconies of RC buildings (Fig. 1) and was conceived to allow the execution of two tests per prototype.

Each prototype has two cantilever type branches of 1.0 m length and a cross-section of 300 mm × 120 mm, continuously connected with a central part also with 1.0 m length and a thicker cross-section, of 300 mm × 200 mm. The bottom reinforcement is composed of 2 bars of 6 mm diameter, and constructive steel stirrups of 6 mm diameter are also applied. Two reinforcement ratios were adopted for the top reinforcement, one composed of 2 steel bars of 8 mm diameter (type A reinforcement) and the other with 2 steel bars of 10 mm diameter (type B reinforcement). The concrete cover thickness of both the top and bottom reinforcements is 30 mm.

The CFRP bar has one extremity with a predefined inclination, which is introduced into a hole executed in the concrete element supporting the balcony (Fig. 3). This inclined extremity is applied according to the ETS technique by using an adhesive to bond the CFRP bar to the surrounding concrete. The other part of the CFRP bar is bonded with an adhesive into a groove executed in the top surface of the RC balcony and, therefore, the NSM technique is used for this part.

Fig. 3 shows, schematically, the strengthening procedure adopted for the series flexurally strengthened with CFRP bars with extremity at 30° and 15°. The strengthening process was initiated by executing two notches on the prototype, approximately 150 mm apart (Fig. 3). The width adopted for the notches was 12 mm and the depth was 15 mm. This notch received the part of the CFRP bar applied according to the

Table 1
Test program with prototypes of RC balconies.

Concrete strength class	Type and percentage of flexural reinforcement	Designation	Age at testing [days]	f_{cm} ** [MPa]
C35	B ρ_{sl} * = 0.44%	C35B-15-1	238	53.8
		C35B-30-1	238	
		C35B-15-2	245	
		C35B-30-2	245	
		C35B-R1	32	38.8
		C35B-R2	46	
	A ρ_{sl} = 0.28%	C35A-15-1	236	46.2
		C35A-30-1	236	
		C35A-R1	47	41.8
		C35A-R2	48	
		C35A-15-2	242	50.9
		C35A-30-2	242	
C25		C25A-R1	51	31.0
		C25A-R2	52	
		C25A-15-1	230	31.4
		C25A-30-1	230	
		C25A-15-2	237	
		C25A-30-2	237	

* $\rho_{sl} = A_{s,top} / \left[300 \times \left(120 - 30 - 6 - \phi_{s,top}/2 \right) \right]$;
** Average compressive strength for cylinder specimens.

NSM technique. The inclined part of the CFRP bar was introduced into a hole with a diameter of 14 mm, according to the ETS technique. The hole was localized in the thicker part of the prototype and started at about 60 mm from the thickness transition section (Fig. 3). Since the CFRP strengthening is not required along the whole length of the cantilever, only about 670 mm of the length was filled with S&P resin 220. The holes were filled with S&P resin 55 and the transition zone was finished off with S&P resin 220. The strengthening process was a two-day task: the NSM portion was executed with Resin 220 in one day, and the ETS portion in the following day with Resin 50. The specimens were deliberately allowed to cure for more than one week before testing to ensure the proper development of the adhesives' properties.

The experimental program was composed of a series of RC balcony prototypes, as indicated in Table 1. It was comprised of two series of different concrete strength classes, C25 and C35, to assess the influence of this property on the effectiveness of the proposed strengthening technique. For evaluating the influence of the flexural tensile reinforcement ratio, ρ_{sl}, on the flexural strengthening effectiveness, the series of concrete strength class C35 was divided into two subseries, one

Table 2
Tensile properties of the steel reinforcements.

| Specimen diameter	10 mm		8 mm		6 mm	
	f_y	f_u	f_y	f_u	f_y	f_u
	[MPa]		[MPa]		[MPa]	
Average	503	608	507	622	579	643
Standard deviation (STD)	21	27	23	15	7	13
Coefficient of variation (CoV)	4%	4%	5%	2%	1%	2%

f_y is the yield stress and f_u is the ultimate stress.

with almost the minimum ρ_{sl} according to the recommendations of *fib* Model Code 2010 [18], $\rho_{sl} = 0.28\%$, abbreviated as reinforcement type A, and another subseries with a conventional percentage for this type of RC structures, $\rho_{sl} = 0.44\%$, abbreviated as reinforcement type B. Each series is constituted by the reference prototype with the acronym CXY-R, where X can be 25 or 35 for identifying the concrete strength class and Y can be A or B to identify the flexural steel reinforcement ratio. The CFRP bars shown in Fig. 3 were used to investigate the influence of the inclination of the ETS portion on the flexural strengthening performance. Preliminary numerical simulations with the model described elsewhere [19] have suggested limiting this inclination to 30° to prevent premature failure in the transition zone of this type of reinforcement.
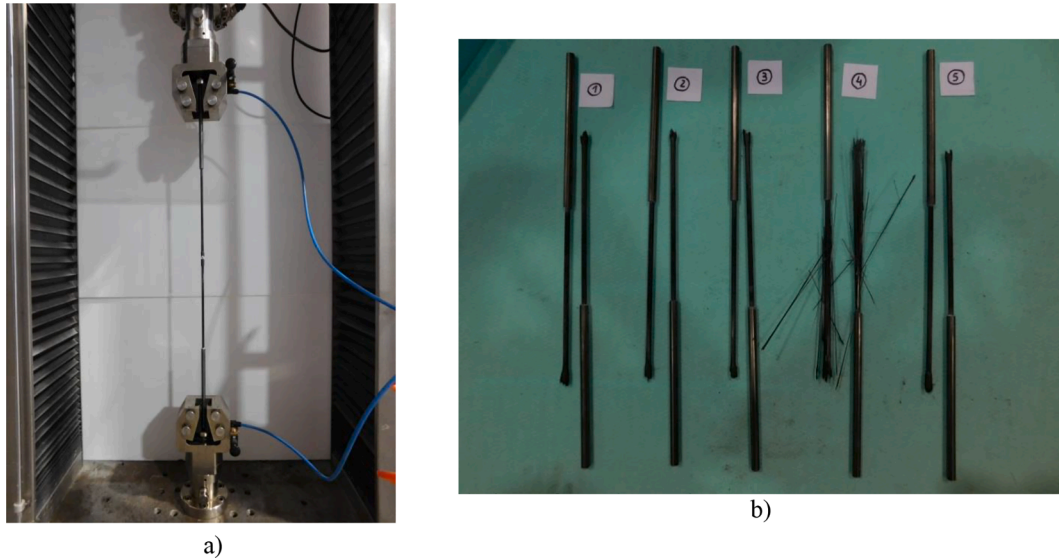
Fig. 4. a) Tensile test of CFRP bar bent at 0°; b) failure modes.
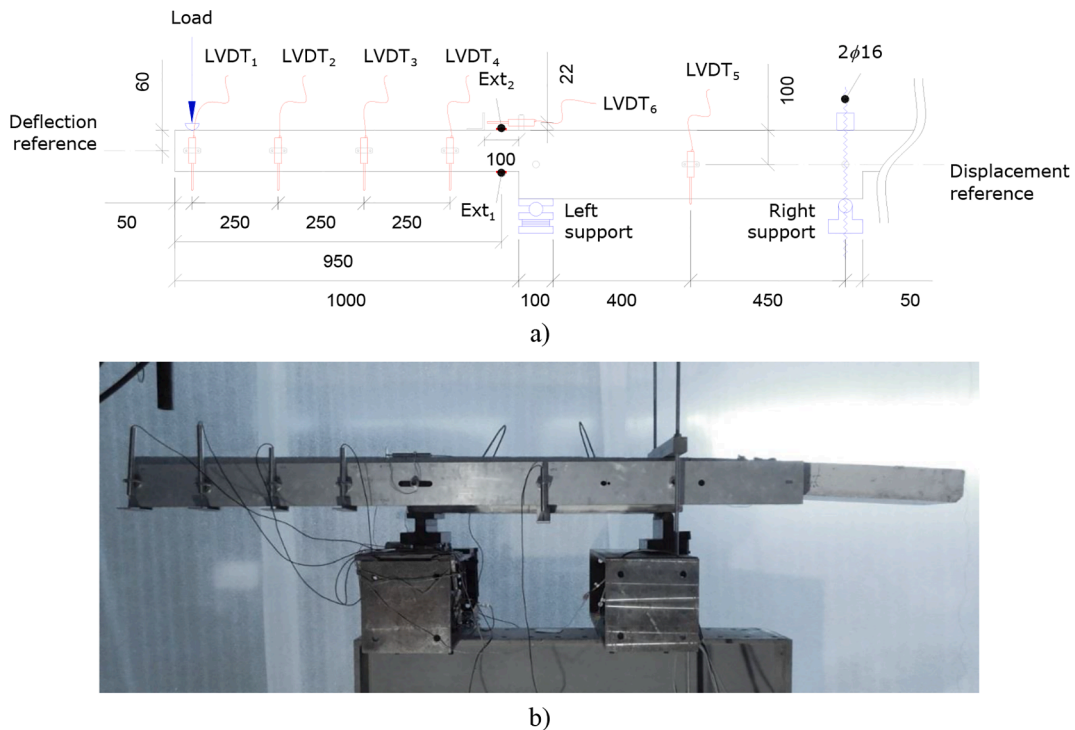
Fig. 5. a) Schematic representation of the load and support conditions, and instrumentation to record the displacements and strains (dimensions in mm); b) aluminium bar supporting the LVDTs for measuring the deflection of the testing region of the prototype.

Therefore, the series of flexurally strengthened prototypes of balconies include tests with CFRP bars with extremities inclined at 15° and 30°. As shown in Fig. 3, each strengthened prototype was strengthened with two of this type of CFRP bars. The strengthened balconies have the acronym CXY-Z, where X and Y have the meaning already indicated, and Z can be 15 or 30, representing the inclination of the extremity of the CFRP bars. For instance, C35A-15 is a test on a balcony prototype of concrete strength class C35, with flexural steel reinforcement type A, and strengthened with CFRP bars with an ETS extremity inclined at 15°. Since two tests were executed for each reference and strengthening configuration, a number is also added to the previous acronyms, for instance: C35A-15–1; C35A-15–2. Therefore, the full experimental program comprises 9 double-sided prototypes and 18 tests, as shown in Table 1.

2.2. Materials properties

The average cylinder compressive strength [20] at the age when the balcony prototypes were tested is indicated in the last column of Table 1. Tensile tests were executed according to the standard [21] on 5 specimens of the types of steel reinforcements adopted in the experimental program, and the relevant results are presented in Table 2.

Tensile tests with 5 CFRP bars of 6 mm diameter were executed according to the recommendations of [22], Fig. 4a. These bars include a small transition zone, although without inclination, since the tensile test setup requires them to be aligned with the tensile load. From these tests, an average tensile strength of 597 MPa with a CoV of 18% was obtained. Fig. 4b shows that only CFRP rod no. 4 exhibited a classic CFRP tensile rupture, producing two specimen halves displaying a bundle of detached fibres.

S&P Resin 220 epoxy adhesive was used to bond the NSM and transition branches of the CFRP bar to the concrete substrate. According to the supplier, the average tensile strength, compressive strength and flexural strength of the adhesive are 15.0, 94.5, 39.5 MPa, respectively, while the elasticity modulus and maximum tensile strain, evaluated by Costa and Barros [23] according to the ISO 527–2 recommendations [24], were 7.4 GPa and 3.0‰, respectively. S&P Resin 55 epoxy adhesive was used for anchoring the ETS branch of the CFRP reinforcement. According to the supplier, the average values of the tensile strength, compressive strength and flexural strength and modulus of elasticity are 15.9, 104.4, 83.2 and 3293 MPa, respectively.

2.3. Loading conditions and monitoring system

The prototype was positioned in the testing frame over two supports positioned 900 mm apart, as depicted in Fig. 5a. Due to the load and support conditions, the upwards movement of the section of the prototype over the external support was restricted by applying a square steel bar (50 mm × 50 mm) transversally at the top of the prototype in that position and fixed to the support with two threaded bars of 16 mm diameter (Fig. 5a).

The five displacement transducers (LVDT1 to LVDT5) measuring the deflection of the testing region of the prototype were supported on an aluminium profile fixed laterally to the middle of the sections over the supports of the prototype to eliminate parasitic measurements of the deflection (Fig. 5b). LVDT6, which was used to monitor a reference length of 100 mm, was used to estimate the strain of the top surface in the extremity of the cantilever part of the prototype. Two strain gauges were installed 50 mm from the end section of the cantilever part of the prototype, one in the bottom face (Ext1) and the other in the top face (Ext2). Loading was applied with a servo-hydraulic jack with 500 kN capacity and controlled by the internal displacement of the actuator, at a constant displacement rate of 0.05 mm/s. The applied load was measured with a load cell of 500 kN capacity.

Table 3
Main results of the reference (unstrengthened) prototype tests.

Prototype's test	δ_{crack}^{Ref} [mm]	P_{crack}^{Ref} [kN]	δ_{yied}^{Ref} [mm]	P_{yied}^{Ref} [kN]	P_{max}^{Ref} [kN]	$P_{l/250}^{Ref}$ [kN]
C25A-R1	0.639	1.075	14.7	4.385	5.225	1.880
C25A-R2	0.593	1.070	16.6	4.580	5.220	2.260
C35A-R1	0.590	1.730	14.0	4.625	5.345	2.535
C35A-R2	0.469	2.000	12.5	4.550	5.435	2.625
C35B-R1	1.017	1.225	16.3	6.505	7.465	2.460
C35B-R2	0.366	1.160	17.2	6.530	7.570	2.900

δ_{crack}^{Ref} and P_{crack}^{Ref} are the displacement and the load at crack initiation, respectively, δ_{yied}^{Ref} and P_{yied}^{Ref} are the displacement and the load at yield initiation, respectively, P_{max}^{Ref} is the maximum load and $P_{l/250}^{Ref}$ is the load at service limit states.

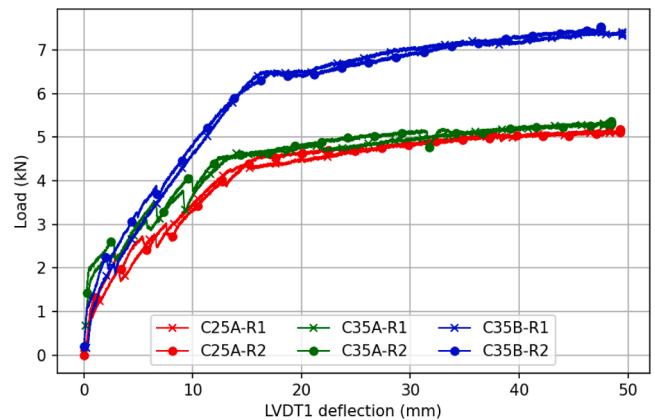Note: δ_{yied}^{Ref} and P_{yied}^{Ref} are determined by tracing the value of 2.5‰ at LVDT6.

Fig. 6. Load versus deflection (LVDT1) in the reference balconies.

Table 4
Cracked length and crack spacing recorded on the reference (unstrengthened) prototype tests.

Prototype's test	Number of cracks		Cracked length [mm]		Average crack spacing [mm]	
	Front	Back	Front	Back	Front	Back
C25A-R1	6	6	480	495	92	97
C25A-R2	7	7	530	495	96	85
C35A-R1	6	5	420	390	90	105
C35A-R2	5	6	335	375	88	100
C35B-R1	7	8	600	565	120	94
C35B-R2	7	7	605	550	111	104

The total cracked length was measured up to the support line.

2.4. Obtained results: Presentation and discussion

2.4.1. Reference prototypes

The main results obtained on the tests with the reference (*Ref*) prototypes (unstrengthened) are summarized in Table 3, while the force *vs* deflection on the LVDT1 is shown in Fig. 6. As expected, prototypes with reinforcement type B exhibited higher load-carrying capacity than prototypes with reinforcement Type A due to the higher flexural-tensile reinforcement ratio. The plots clearly exhibit a linear branch up to crack initiation with the highest stiffness, followed with an elasto-cracked stage of smaller stiffness due to the crack formation and propagation up to the yield initiation of the top reinforcement, and a final stage with a much smaller stiffness where the reinforcement is yielded and where a certain hardening is visible, mainly due to the tensile hardening behaviour of this reinforcement. As predicted, all prototypes tended to move upwards, but the supporting conditions provided to the
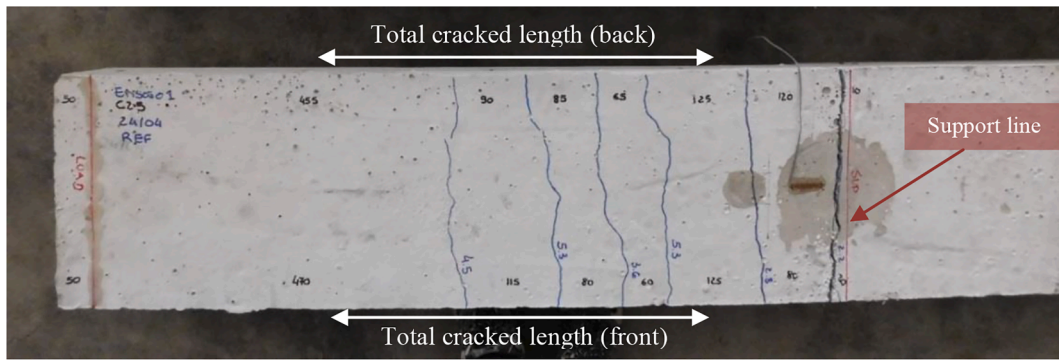
Fig. 7. Concept of cracked length in the tested prototypes, with the localization of the support line.

Table 5
Relevant results of the strengthened balcony prototypes.

Prototype's test	δ_{crack}^{Str} [mm]	P_{crack}^{Str} [kN]	δ_{yied}^{Str} [mm]	P_{yied}^{Str} [kN]	P_{max}^{Str} [kN]	$P_{l/250}^{Str}$ [kN]	$\varepsilon_{f,Rup}$ [‰]	$f_{f,Rup}$ [MPa]
C25A-15-1	1.532	2.930	15.12	7.795	11.030	4.030	8.06	1290
C25A-15-2	1.424	2.700	18.95	8.865	10.390	4.105	6.75	1080
C25A-30-1	1.730	3.115	14.85	7.250	8.165	3.890	4.69	750
C25A-30-2	1.460	2.425	15.42	7.215	8.590	3.600	5.50	880
C35A-15-1	2.183	3.495	15.42	8.055	10.940	4.410	7.50	1200
C35A-15-2	1.610	3.435	13.81	7.675	9.965	4.425	6.75	1080
C35A-30-1	1.657	3.480	16.36	8.070	9.795	4.425	6.88	1100
C35A-30-2	1.791	3.405	15.98	8.100	10.850	4.120	8.12	1300
C35B-15-1	2.347	4.105	12.93	9.890	14.800	5.445	9.00	1440
C35B-15-2	–	–	–	–	–	–	–	–
C35B-30-1	1.980	4.350	16.15	9.415	10.910	5.080	6.25	1000
C35B-30-2	1.500	3.525	12.64	8.485	11.260	5.005	5.62	900

δ_{crack}^{Str} and P_{crack}^{Str} are the displacement and the load at crack initiation, respectively, δ_{yied}^{Str} and P_{yied}^{Str} are the displacement and the load at yield initiation, respectively, P_{max}^{Str} is the maximum load, and $P_{l/250}^{Str}$ is the load at service limit states., $\varepsilon_{f,Rup}$ and $f_{f,Rup}$ are the tensile strain and stress, respectively, in the CFRP at its rupture.

outer support were efficient to limit this movement to a negligible value (less than 0.20 mm).

In all tested reference balconies, the crack pattern was generally similar, exhibiting an average crack spacing of about 100 mm at stabilized crack propagation stage (see Table 4 and Fig. 7). Average crack spacing was evaluated by dividing the number of cracks formed on the top surface of a prototype by the length of this cracked region. In the series with the same reinforcement ratio, the total cracked length decreased with the increase of concrete quality. Moreover, in the series of equal concrete strength classes, the total cracked length increased with the increase of the reinforcement ratio. In both cases, these observations are justified by the higher load carrying capacity when the concrete strength class and flexural reinforcement ratio increase.

2.4.2. Strengthened prototypes

The relevant results obtained in the strengthened (*Str*) balcony prototypes are indicated in Table 5. The recording data file corresponding to the test of C35B-15-2 was corrupted and, therefore, no load/displacements/strains can be presented for this test. However, based on the load levels indicated in this prototype for recording the force *vs* crack propagation history, its maximum load was very close to the one registered in the C35B-15-1.

By considering the compressive and tensile strains recorded in Ext1 and LVDT6, respectively, and assuming a linear interpolation for obtaining the tensile strain at the level of the CFRP bars, the tensile strains at their rupture (when an abrupt load decay was observed in the force–deflection response) are indicated in Table 5, $\varepsilon_{f,Rup}$. For the linear interpolation, it was considered that the axis of the LVDT6 was 22 mm

Table 6
Flexural strengthening performance indicators registered in the balcony prototypes.

Strengthened prototype	$\overline{P}_{crack}^{Str}$ [kN]	$\overline{P}_{yied}^{Str}$ [kN]	$\overline{P}_{max}^{Str}$ [kN]	$\overline{P}_{l/250}^{Str}$ [kN]	Reference prototype				$\Delta\overline{P}_{crack}$ [%]	$\Delta\overline{P}_{yield}$ [%]	$\Delta\overline{P}_{max}$ [%]	$\Delta\overline{P}_{l/250}$ [%]
					$\overline{P}_{crack}^{Ref}$ [kN]	$\overline{P}_{yied}^{Ref}$ [kN]	$\overline{P}_{max}^{Ref}$ [kN]	$\overline{P}_{l/250}^{Ref}$ [kN]				
C25A-15	2.815	8.330	10.710	4.068	1.073	4.483	5.223	2.070	162.5	85.8	105.1	96.5
C25A-30	2.770	7.233	8.378	3.745					158.3	61.3	60.4	80.9
C35A-15	3.465	7.865	10.453	4.418	1.865	4.588	5.390	2.580	85.8	71.4	93.9	71.2
C35A-30	3.443	8.085	10.323	4.273					84.6	76.2	91.5	65.6
C35B-15	4.105	9.890	14.800	5.445	1.193	6.518	7.518	2.680	244.2	51.7	96.9	103.2
C35B-30	3.938	8.950	11.085	5.043					230.2	37.3	47.5	88.2

$\overline{P}_{crack}^{Str/Ref}$ is the average load at crack initiation, $\overline{P}_{yied}^{Str/Ref}$ is the average load at yield initiation, $\overline{P}_{max}^{Str/Ref}$ is the average maximum load applied on the cantilever, $\overline{P}_{l/250}^{Str/Ref}$ is the average load at service limit states, $\Delta\overline{P}_{crack} = \left(\overline{P}_{crack}^{Str} - \overline{P}_{crack}^{Ref}\right)\Big/\overline{P}_{crack}^{Ref}$, $\Delta\overline{P}_{yield} = \left(\overline{P}_{yield}^{Str} - \overline{P}_{yield}^{Ref}\right)\Big/\overline{P}_{yield}^{Ref}$, $\Delta\overline{P}_{max} = \left(\overline{P}_{max}^{Str} - \overline{P}_{max}^{Ref}\right)\Big/\overline{P}_{max}^{Ref}$ and $\Delta\overline{P}_{l/250} = \left(\overline{P}_{l/250}^{Str} - \overline{P}_{l/250}^{Ref}\right)\Big/\overline{P}_{l/250}^{Ref}$ are the percentage increase of the average load at crack initiation, yield initiation, maximum load and service limit states, respectively.
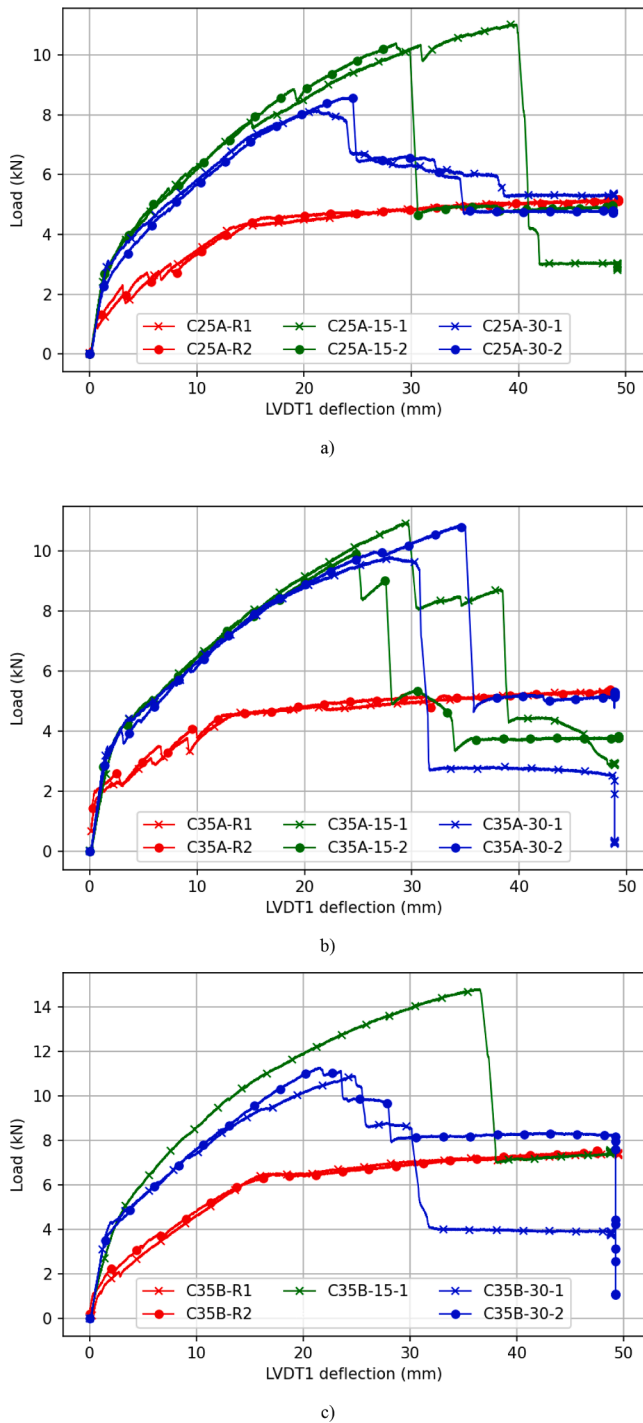
a)

b)

c)

Fig. 8. Comparison of load versus deflection (LVDT1) recorded in the reference and corresponding strengthened series: a) C25A, b) 35A, c) and C35B.

above the top surface of the prototype and the geometric centre of the CFRP bar was at the middle depth of the notch (7.5 mm below that surface), Fig. 5. For determining the corresponding CFRP tensile stress, the nominal elastic modulus of the bar was considered ($E_f = 160$ GPa), and the obtained values are also indicated in Table 5. Due to the still manual production of the CFRP bars applied in the balcony prototypes, relatively high dispersion of the strain at their rupture was obtained, but it is confirmed that the $\varepsilon_{f,Rup}$ was smaller in the CFRP reinforcements with an extremity at 30° (in average, $\varepsilon_{f,Rup} = 7.61$‰ in the series with extremities at 15° and $\varepsilon_{f,Rup} = 6.18$‰ in the series with extremities at 30°). These values provide tensile strength values that are higher than

the values registered in the control tensile tests with specimens of these bars (average value of 597 MPa with a COV of 18%). This can be justified by the distinct length of the transition zone of the specimens tested in uniaxial tension and of the CFRP bars applied in the balcony prototypes. The former specimens had smaller, and therefore more abrupt transition length, which may have penalized the force transference mechanism between the bar portions on each side of the transition zone, reducing their tensile strength in comparison to the CFRPs used in the balcony prototypes.

In Table 6, a general analysis of the results is presented. Overall, the load at crack initiation of the strengthened prototypes was considerably higher than the one registered in the corresponding reference prototypes. This increase on the P_{crack} ($\Delta\overline{P}_{crack} = \left(\overline{P}_{crack}^{Str} - \overline{P}_{crack}^{Ref}\right)\Big/\overline{P}_{crack}^{Ref}$) is mainly justified by the concrete age difference when the reference and strengthened prototypes were tested, about 50 days and 250 days, respectively. Regarding the increase of load at service limit states ($\Delta\overline{P}_{l/250} = \left(\overline{P}_{l/250}^{Str} - \overline{P}_{l/250}^{Ref}\right)\Big/\overline{P}_{l/250}^{Ref}$, load at deflection of $l/250$, where l = 1000 mm and corresponds to the length of the cantilever part of the balcony) and at maximum load ($\Delta\overline{P}_{max} = \left(\overline{P}_{max}^{Str} - \overline{P}_{max}^{Ref}\right)\Big/\overline{P}_{max}^{Ref}$) due to the adopted strengthening configurations, both were observed to be the most significant. In both cases, $\Delta\overline{P}_{l/250}$ and $\Delta\overline{P}_{max}$, the load increase was always higher on the prototypes strengthened with CFRP bars bent at 15° than on the corresponding prototypes strengthened with bars bent at 30°. As an example, it can be referred that the CFRP bars bent at 15° produced an average increase of 90% for the $\overline{P}_{l/250}$ and 99% for the $\overline{P}_{max}$. On the other hand, CFRP bars bent at 30° provided an average increase of 78% for the $\overline{P}_{l/250}$ and 67% for the $\overline{P}_{max}$. It becomes evident that the larger the bend angle, the lower the contribution of the CFRP bar for the ultimate load capacity, which was justified by the $\varepsilon_{f,Rup}$ already indicated in Table 5.

Fig. 8 compares the force *vs* deflection at LVDT1 for the reference and strengthened prototypes.

Fig. 9 shows typical crack patterns at the failure of the strengthened prototypes. It is realized that the main failure crack is localized at the section of the transition zone of the CFRP bars, and progressed towards the corner of the connection between the two parts of different thicknesses forming the prototype. As occurred in the reference prototypes, the strengthened prototypes have failed in bending, since at their maximum load-carrying capacity, the strains in the existing steel reinforcement have already exceeded their yield strain. In the strengthened prototypes, the CFRP have, in general, ruptured in their transition zone.

Table 7 presents the cracked length and crack spacing measured in the tested strengthened balcony prototypes. While in terms of cracked length, no significant difference is observed between these prototypes and the corresponding reference ones, in the crack spacing a significant difference is identified. It was observed that the spacing between cracks decreased from about 100 mm (roughly 80% of the cantilever cross-section height) in the reference balconies to about 65 mm (about 55% of the cantilever cross-section height) in the strengthened balconies.

3. Numerical simulations

3.1. Predictions according to the fib bulletin 90

For the present RC elements, the critical section in terms of flexural capacity is the extremity of the cantilever closest to the support. In this section, the design value of the resisting bending moment, M_{Rd}, should be higher or equal to the maximum design value of the actuating bending moment, M_{Sd}. According to the *fib* bulletin 90 [17], the M_{Rd} is limited by the maximum possible design value of the tensile stress in the FRP (provided that the concrete compressive strain does not exceed the concrete crushing strain, $\varepsilon_{cu} = 0.0035$):
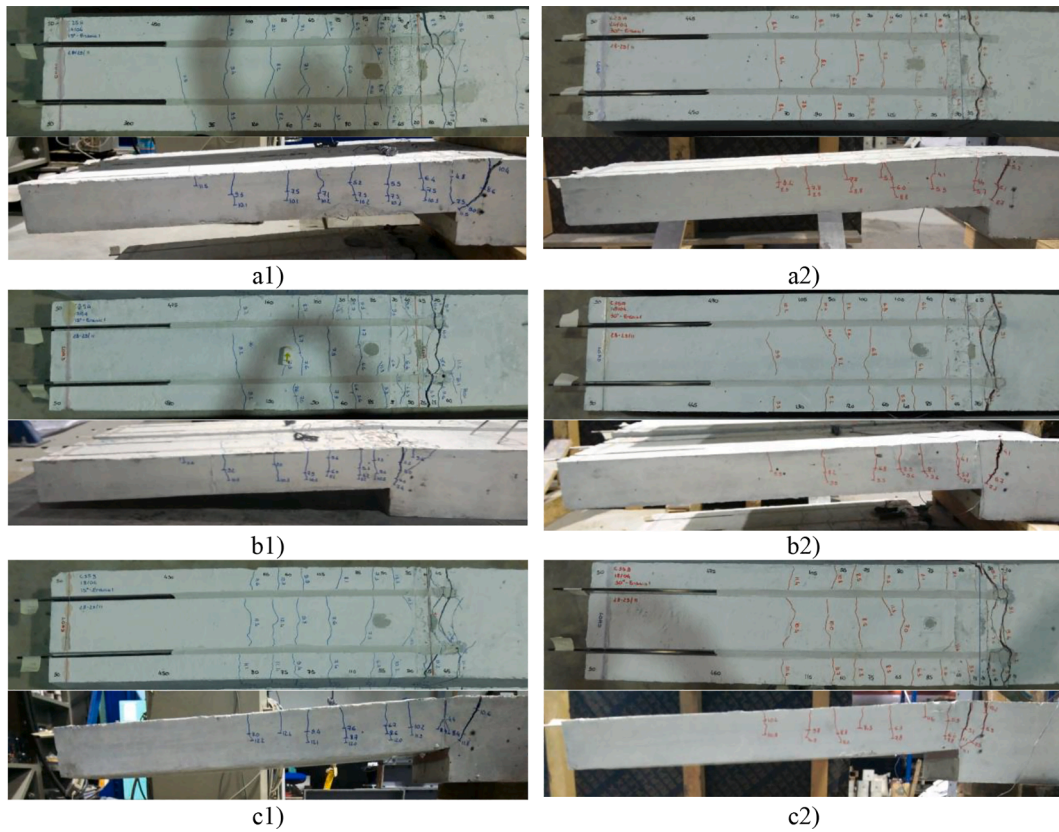
Fig. 9. Representative crack patterns in the flexurally strengthened tested balcony prototypes of series: a) C25A (a1: C25A-15–1; a2: C25A-30–1); b) C35A (b1: C35A-15–1; b2: C35A-30–1); c) C35B (c1: C35B-15–1; c2: C35B-30–1).

Table 7
Cracked length and crack spacing on the strengthened prototype tests.

Prototype's test	Number of cracks		Cracked length [mm]		Average crack spacing [mm]	
	Front	Back	Front	Back	Front	Back
C25A-15-1	10	10	590	500	68	61
C25A-15-2	7	8	470	475	74	62
C25A-30-1	7	7	500	505	76	66
C25A-30-2	9	9	460	440	60	54
C35A-15-1	9	9	470	475	64	58
C35A-15-2	8	9	470	440	71	54
C35A-30-1	7	8	505	480	77	68
C35A-30-2	10	6	515	450	56	81
C35B-15-1	8	8	500	460	71	64
C35B-15-2	7	8	480	515	73	69
C35B-30-1	10	9	490	475	56	61
C35B-30-2	8	7	480	490	65	81

The total cracked length was measured up to the support line.

$$\sigma_{fd} = min\left(f_{fbd,IC} \quad f_{fd}\right) \tag{1}$$

where

$$f_{fbd,IC} = \frac{1}{\gamma_{fb}}\sqrt{\frac{2E_f G_f p_f}{A_f}} \tag{2}$$

is the design value of the tensile stress due to the occurrence of an intermediate crack induced debonding (IC), and

$$f_{fd} = n_f \frac{f_{fk}}{\gamma_f} \tag{3}$$

is the design value of the FRP tensile strength, being $\gamma_{fb} = 1.3$, $\gamma_f = 1.25$

and $n_f = 0.8$. In Eq. (2) E_f, $p_f = \pi\phi_f$, $A_f = \pi\phi_f^2/4$ are the elasticity modulus, perimeter and cross-section area of an FRP reinforcement, being ϕ_f its diameter (in the present case 6 mm), and:

$$G_f = \frac{\tau_{b1d}\ s_{0d}}{2} \tag{4}$$

is the fracture energy of the FRP-substrate interface, where τ_{b1d} and s_{0d} are the bond strength and the ultimate slip of the rigid-softening bond stress vs slip constitutive law that governs the bond behaviour between an NSM FRP reinforcement and its surrounding concrete substrate. The design value of the bond strength can be obtained from the relevant properties of the adopted adhesive and concrete substrate, namely:

$$\tau_{b1d} = \frac{1}{\gamma_{fb}}min\left(a_{ba}\tau_{bak} \quad a_{bc}\tau_{bck}\right) \tag{5}$$

where

$$\tau_{bak} = K_{sys}\sqrt{\left[2f_{atk} - 2\sqrt{f_{atk}^2 + f_{ack}f_{atk}} + f_{ack}\right]f_{atk}} \tag{6}$$

$$\tau_{bck} = K_{bck}\sqrt{f_{cm}} \tag{7}$$

and $a_{ba} = 0.5$ and $a_{bc} = 0.9$. In Eq. (6) f_{atk} and f_{ack} are the characteristic value of the tensile and compressive strength of the adhesive, respectively, while K_{sys} is a product-specific factor for adhesive bond failure by testing approvals (=0.6 for pre-design). Eq. (7) K_{bck} is a product-specific factor for concrete bond failure by testing approvals (=4.5 for pre-design) and f_{cm} is the concrete average compressive strength.

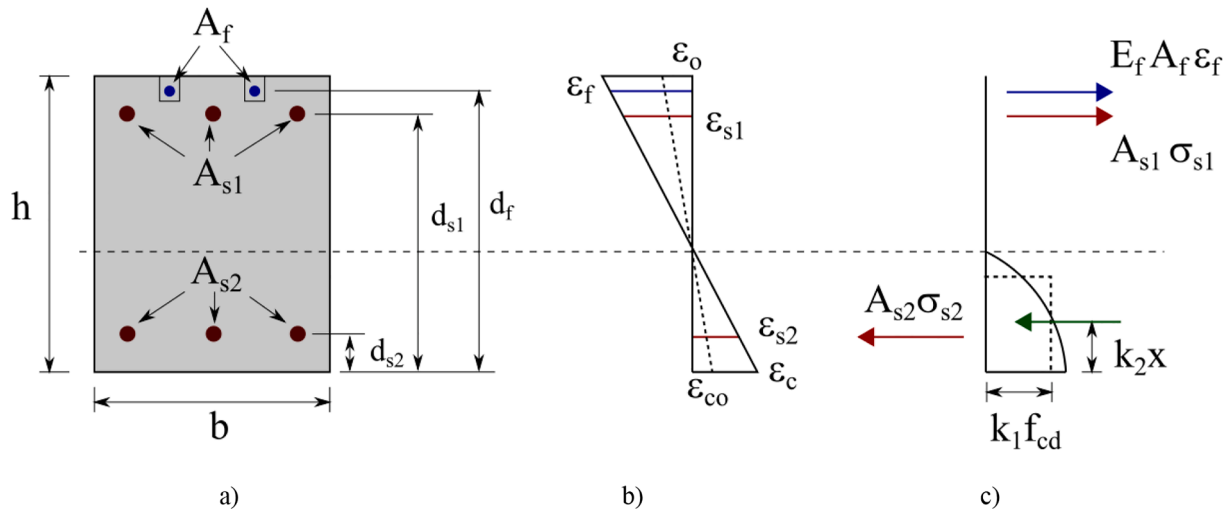The effective bond length is obtained from:

Fig. 10. a) Cross-section, b) Strain profile in the cross-section with the initial strain in the concrete substrate when FRP will be applied, ε_o; c) internal forces in the cross-section for the strengthening scenario.

$$l_e = \pi s_{0d} \sqrt{\frac{2A_f E_f}{8G_f p_f}} \tag{8}$$

The strain in the concrete substrate where FRP will be applied, ε_o, should be estimated for the applied bending moment at the strengthening stage, M_o:

$$\varepsilon_o = \frac{M_o(h - x_o)}{E_{cm}I_o} \tag{9}$$

where E_{cm} is the average value of the concrete Young's modulus, determined from f_{cm} (in the present case from the values of the last column of Table 1) according to the recommendations of MC2010 [18], and x_o is the depth of the neutral axis obtained by solving the following equation, Fig. 10:

$$\frac{1}{2}bx_o^2 + (\eta_s - 1)A_{s2}(x_o - d_{s2}) - \eta_s A_{s1}(d_{s1} - x_o) = 0 \tag{10}$$

In this equation $\eta_s = E_s/E_{cm}$ is the modular ratio of the steel, b is the width of the cross-section, A_{s2} and d_{s2} are the cross-section area and the depth of the steel reinforcement in the compression zone, A_{s1} and d_{s1} are the cross-section area and the depth of the steel reinforcement in the tension zone. In Eq. (9), I_o is the moment of inertia of the cracked section:

$$I_o = \frac{1}{3}bx_o^3 + (\eta_s - 1)A_{s2}(x_o - d_{s2})^2 + \eta_s A_{s1}(d_{s1} - x_o)^2 \tag{11}$$

and if M_o is less than the cracking moment of the section, M_{cr}:

$$M_{cr} = k_{fl}f_{ctm}W_{co} \tag{12}$$

$$k_{fl} = max\left[1.6 - \frac{h}{1000} \quad 1\right] \quad (h \text{ in mm}) \tag{13}$$

$$W_{co} = \frac{bh^2}{6} \tag{14}$$

the uncracked moment of inertia of the section, $I_o = (bh^3)/12$ where h is the height of the cross-section, should be used in Eq. (9). In Eq. (12) f_{ctm} is the concrete average tensile strength, determined from f_{cm} (in the present case from the values of the last column of Table 1) according to the recommendations of MC2010 [18].

For determining the resisting bending moment of the strengthened RC element, M_{Rd}^{Str}, the depth of the neutral axis, x, is determined iteratively by solving the following force equilibrium equation (see Fig. 10):

$$k_1[\varepsilon_c(x)]f_{cd}2k_2[\varepsilon_c(x)]xb + \sigma_{s2}(x)A_{s2} - \sigma_{s1}(x)A_{s1} - \sigma_{fd}A_f = 0 \tag{15}$$

where

$$k_1(\varepsilon_c) = 8 \times 10^6[\varepsilon_c(x)]^3 - 108749[\varepsilon_c(x)]^2 + 519.12\varepsilon_c(x) \quad \text{for } 0 < \varepsilon_c \leqslant \varepsilon_{cu} \tag{16}$$

$$k_2(\varepsilon_c) = 2036.3[\varepsilon_c(x)]^2 + 17.789\varepsilon_c(x) + 0.3314 \quad \text{for } 0 < \varepsilon_c \leqslant \varepsilon_{cu} \tag{17}$$

Table 8
Experimental versus predictions according to the *fib* bulletin 90.

| Prototype's test	f_{cm} (MPa)	ε_o	M_{cr} (kN.m)	l_e (mm)	σ_{fd} (MPa)	ε_f (‰)	ε_c (‰)	ε_{s2} (‰)	σ_{s2} (MPa)	ε_{s1} (‰)	σ_{s1} (MPa)	x (mm)	M_R^{Str} (kN.m)	$F_{R.Ana}^{Str} = \frac{M_R^{Str}}{0.95}$ (kN)	$F_{R.Exp}^{Str}$ (kN)	$\frac{F_{R.Exp}^{Str}}{F_{R.Ana}^{Str}}$
C25A-15	31.4	7.37	3.2	278	904	5.6	−2.1	−0.9	−175	4.0	507	27	9.41	9.91	10.71	1.08
C25A-30–1		$\times 10^-$			750	4.7	−1.7	−0.7	−146	3.3	507	28	8.43	8.87	8.16	0.92
C25A-30–2		5			880	5.5	−2.0	−0.9	−170	3.9	507	27	9.26	9.74	8.59	0.86
C35A-15–1	46.2	6.96	4.1		904	5.6	−1.7	−1.1	−219	4.0	507	24	10.06	10.59	10.94	1.03
C35A-30–1		$\times 10^-$													9.80	0.93
		5														
C35A-15–2	50.9	6.86	4.4		904	5.6	−1.6	−1.1	−230	4.1	507	23	10.27	10.81	9.96	0.88
C35A-30–2		$\times 10^-$													10.85	1.00
		5														
C35B-15–1	53.8	5.76	4.6		904	5.6	−1.7	−1.1	−211	3.9	503	24	11.91	12.54	13.50	1.08
C35B-30–1		$\times 10^-$			904	5.6	−1.7	−1.1	−211	3.9	503	24	11.91	12.54	10.91	0.87
C35B-30–2		5			900	5.6	−1.7	−1.1	−211	3.9	503	24	11.88	12.20	11.26	0.90
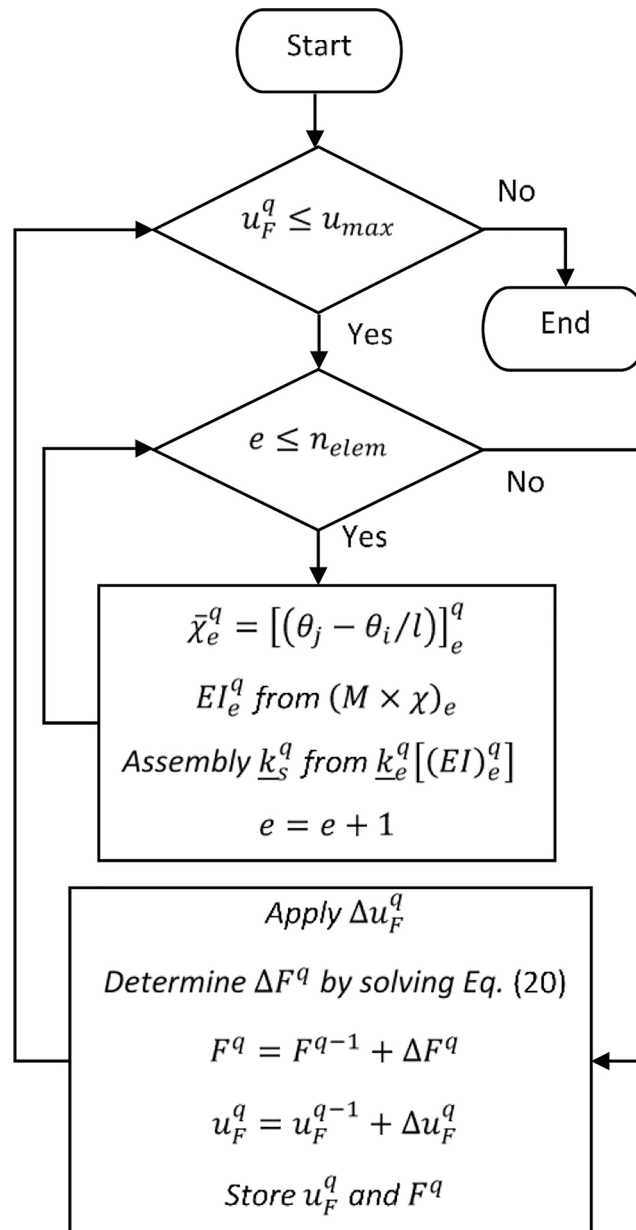
Fig. 11. Flowchart for the proposed numerical approach to simulate the force–deflection of the prototypes failing in bending.
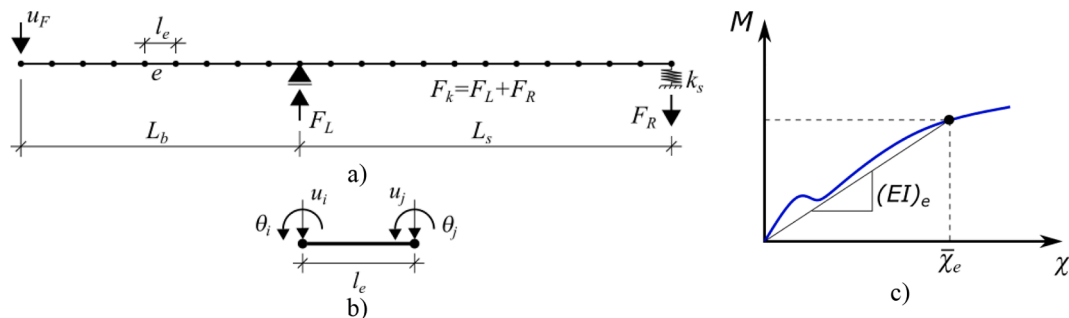

Fig. 12. a) Structural model, b) element representation and its degrees of freedom, c) M-χ relationship.
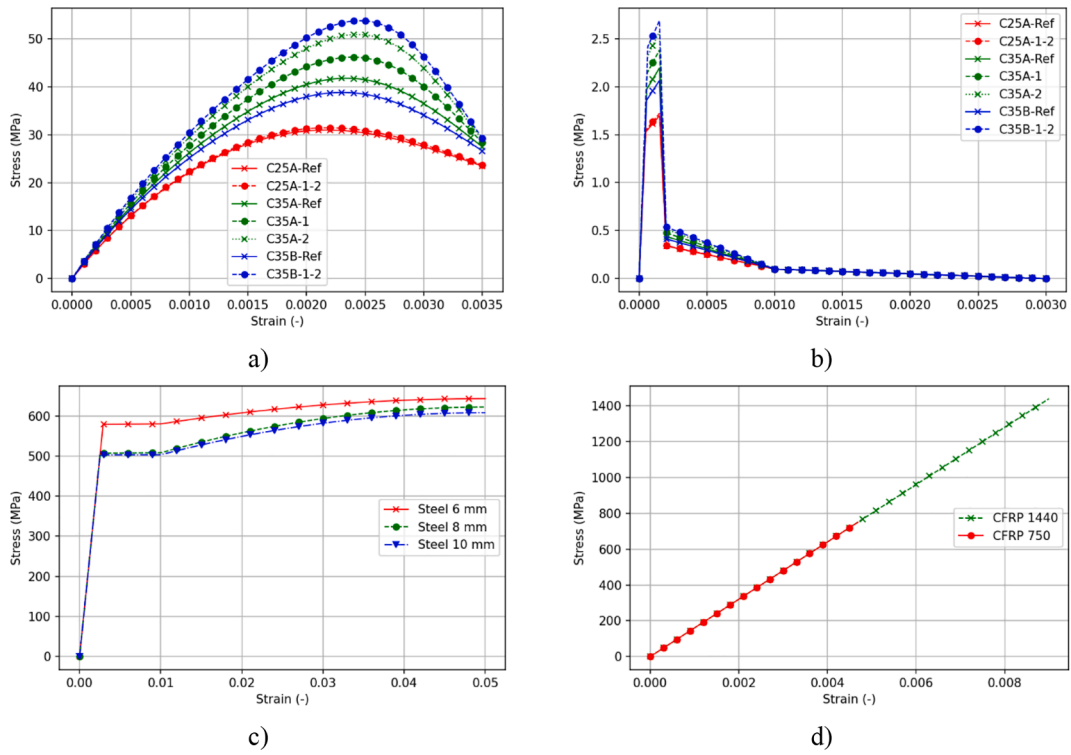
Fig. 13. Stress–strain diagram to obtain the M-χ relationship for each different cross-section: a) Concrete in compression, b) Concrete in tension, c) Steel, d) CFRP.

$$\varepsilon_f = \varepsilon_{fd} = \frac{\sigma_{fd}}{E_f} \tag{18}$$

$$\varepsilon_c(x) = \left(\varepsilon_{fd} + \varepsilon_o\right) \frac{x}{d_f - x} \leqslant \varepsilon_{cu} \tag{19}$$

$$\varepsilon_{s2}(x) = \left(\varepsilon_{fd} + \varepsilon_o\right) \frac{x - d_{s2}}{d_f - x}; \quad \sigma_{s2}(x) = min\left[\,\varepsilon_{s2}(x)E_s \quad f_{yd}\,\right] \tag{20}$$

$$\varepsilon_{s1}(x) = \left(\varepsilon_{fd} + \varepsilon_o\right) \frac{d_{s1} - x}{d_f - x}; \quad \sigma_{s1}(x) = min\left[\,\varepsilon_{s1}(x)E_s \quad f_{yd}\,\right] \tag{21}$$
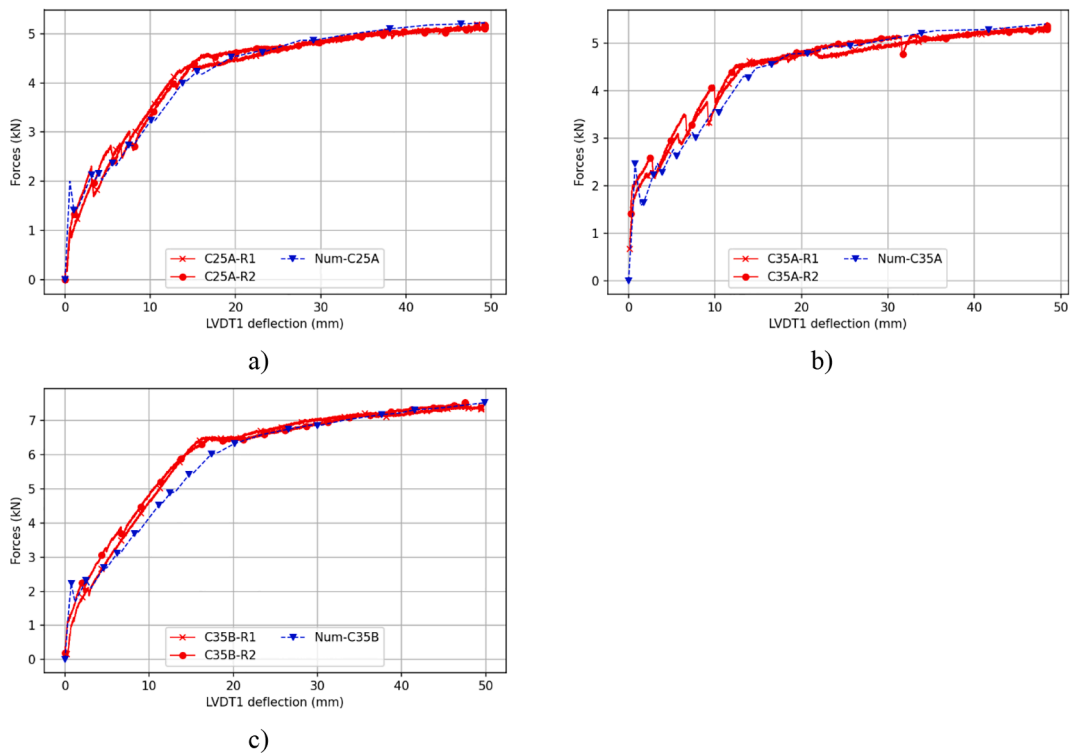

Fig. 14. Simulation of the force–deflection of the reference balcony prototypes of series: a) C25A, b) C35A, and c) C35B.
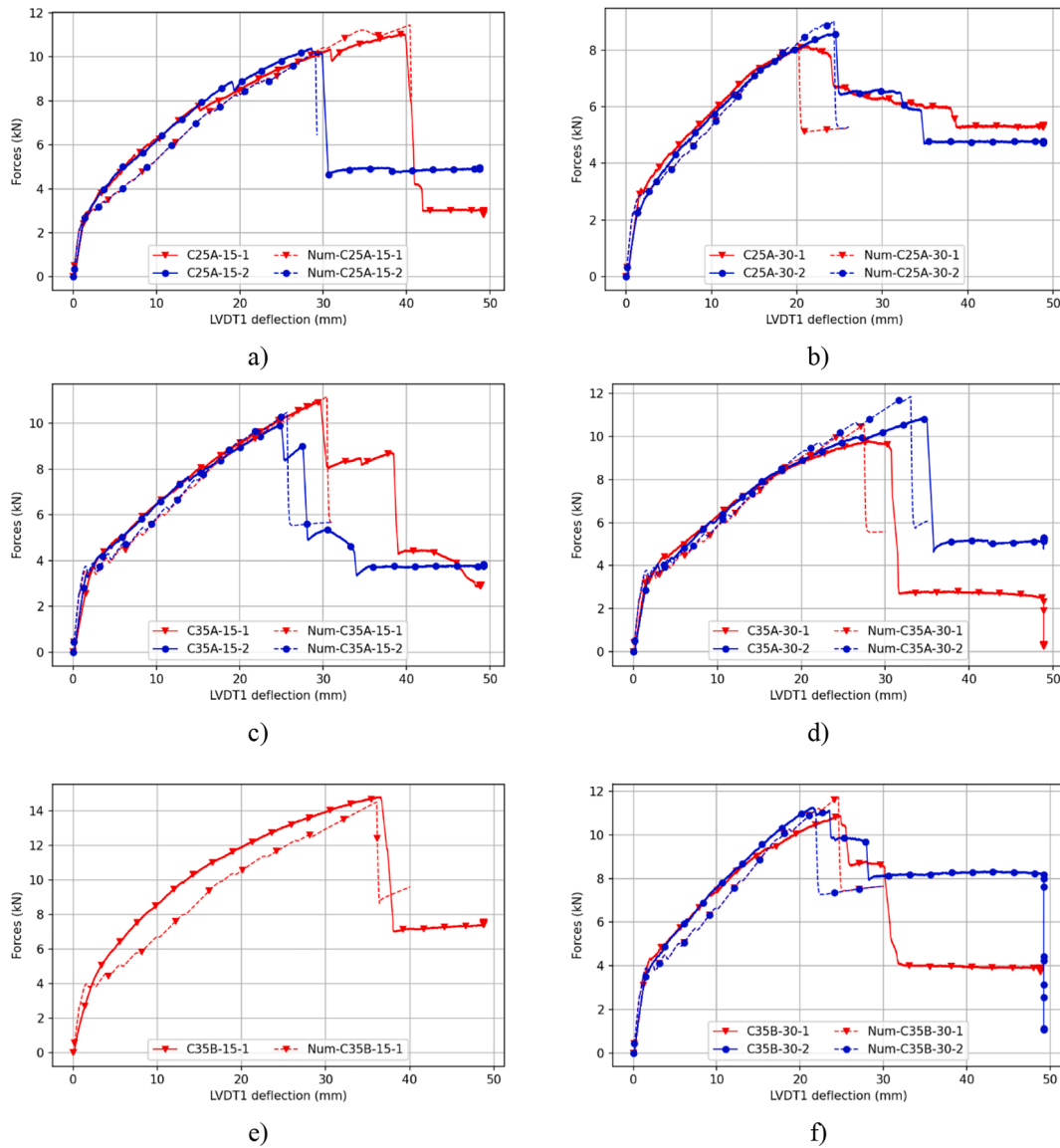
Fig. 15. Simulation of the force–deflection of the strengthened balcony prototypes of series: a) C25A-15 b) C25A-30 c) C35A-15 d) C35A-30 e) C35B-15 f) C35B-30.

being d_f the internal arm of the FRP. After obtaining x, the resisting bending moment is determined from the following equation:

$0.12m \times 0.3m \times 24kN/m^3 = 0.86kN/m \implies M_0 = = 0.86 \times 1^2/2 = 0.43kN.m$), considering the average values obtained experimentally for the properties of the intervenient materials (steel bars, CFRP bars and

$$M_{Rd}^{Str} = \sigma_{s1}(x)A_{s1}\{d_{s1} - k_2[\varepsilon_c(x)]x\} + \sigma_{s2}(x)A_{s2}\{k_2[\varepsilon_c(x)]x - d_{s2}\} + \sigma_{fd}A_f\{d_f - k_2[\varepsilon_c(x)]x\} \tag{22}$$

For evaluating G_f it is necessary to know s_{0d}. Since this information is not yet available for the used CFRP bars, it was estimated by considering the experimental results obtained previously in CFRP rods of 8 mm diameter and smooth surface [25], where $s_{0d} \cong 1.0$ mm was registered. For determining τ_{b1d} according to Eq. (5), the compressive and tensile strengths indicated in the datasheet of the supplier of the adhesive applied in both the NSM and transition parts of the CFRP were adopted.

The M_{Rd}^{Str} of the strengthened prototypes and corresponding applied load, $F_{Rd}^{Str} = M_{Rd}^{Str}/0.95$, were determined by assuming the CFRP was installed when only the dead weight of the balcony, pl, was applied ($pl =$

concrete), and using $\gamma_c = \gamma_s = \gamma_{fb} = \gamma_f = n_f = 1.0$. Regarding the adhesive, the properties were adopted as given by the supplier, $f_{acm} = 94.5$ MPa, $f_{atm} = 15.0$ MPa. The results are presented in Table 8. The obtained results show that *fib* bulletin 90 has provided an average $F_{R,Exp}^{Str}/F_{R,Ana}^{Str}$ of 0.95 and STD of 0.08.

3.2. Developed approach for design RC cantilever type structures according to the proposed strengthened technique

This section proposes a numerical approach of fast and simple use to estimate the force–deflection of the tested RC balcony prototypes, with potentialities of being applied in real design scenarios. The results of the
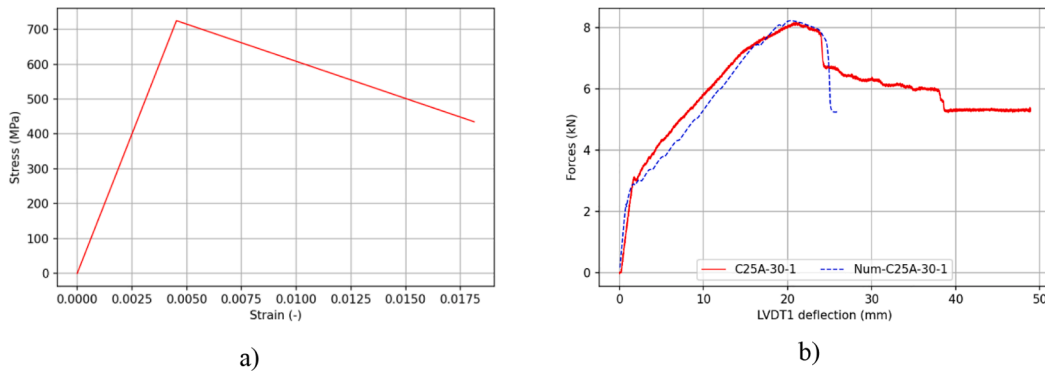
a)

b)

Fig. 16. a) Bilinear stress–strain diagram for simulating the CFRP bars of series C25A-30; b) Simulation of the force–deflection of the series C25A-30.

reference and strengthened balconies tested in the experimental program of this research were used to evaluate the predictive performance of the proposed numerical approach.

The force–deflection response of statically determined balcony prototypes failing in bending is determined according to the algorithm described in the flowchart in Fig. 11. A balcony prototype is discretized by 2D Bernoulli beam elements (e) of length l_e, as showed Fig. 12a. The boundary conditions applied to the structural model comprise a roller at end of the first span (left support) and a spring at the end of the second span (right support) for simulating the 2 Ø 16 mm rebar used in the test setup (Fig. 5a). For each increment of displacement (Δu_F^q) at the loaded section of a given loading step q, the algorithm determines the updated stiffness of the entire specimen ($\underline{K}_S^q$) by assembling the updated stiffness matrix of each Bernoulli beam element ($\underline{K}_e^q[(EI)_e^q]$), where $(EI)_e^q$ is the secant flexural stiffness of the element e determined from the moment–curvature of the representative cross-section of this element, $(M - \chi)_e$, Fig. 12c. This $(EI)_e^q$ is determined by evaluating the average curvature of the element, by considering the rotations of the two nodes of the element, $\overline{\chi}_e^q = [(\theta_j - \theta_i)/l]_e^q$, Fig. 12b. By substitution in the system of equilibrium equations, $\underline{K}_S^q \Delta \underline{u}_S^q = F_S^q$, it is possible to determine directly the ΔF^q from the imposed incremental displacement:

$$\begin{bmatrix} \Delta F \\ \Delta R \end{bmatrix}^q = \left\{ \underline{K}_{S,pp}^q - \underline{K}_{S,pf}^q \left[\underline{K}_{S,ff}^q \right]^{-1} \underline{K}_{S,fp}^q \right\} \begin{bmatrix} \Delta u_F^q \\ 0 \end{bmatrix} \quad (20)$$

where the subscripts p and f represent the prescribed and the free degrees of freedom of the structure. The pair $(u_F \quad F)^q$ is then stored for plotting the $u_F - F$ curve at the end of the analysis.

The $M - \chi$ relationship was implemented using the concept of cross-section decomposed into layers. Using this concept, the thickness and width of each layer are defined by the user based on the cross-section geometry. The model assumes a perfect bond between the materials, a linear strain profile, and that the section remains plane after deformation. For obtaining a point of $M - \chi$, the neutral axis is determined for an imposed strain increment in a control layer, by considering the axial force equilibrium in the cross-section, complying with the constitutive laws of the materials and the geometry of the layers. After attaining this force equilibrium, the curvature can be obtained as the ratio of the strain in a certain layer and its distance to the neutral axis, while the corresponding bending moment is determined from the internal arm of the force installed in each layer. More details can be found elsewhere [26].

The concrete properties and the tensile stress–strain relations shown in Fig. 13a and Fig. 13b, adopted in the numerical simulations, were determined according to the recommendations of *fib* MC2010 [15] by considering the f_{cm} values indicated in Table 1, obtained experimentally. The stress–strain relations for the 6, 8 and 10 mm diameter's steel bars are presented in Fig. 13c. A linear stress–strain relation was adopted to simulate the CFRP bars. Fig. 13d illustrates the minimum and maximum CFRP strength values experimentally obtained in the different tests (see

Table 5 $f_{f,Rup}$).

Fig. 14 compares the force–deflection ($u_F - F$) registered experimentally and obtained numerically for the reference prototypes, where good predictive performance is demonstrated. The load decays observed during the cracking propagation stage were captured by the model, as well as the load at yield initiation, and the maximum deviation on the ultimate load was 2%, 1% and 1% for the reference prototypes C25A, C35A and C35B, respectively.

Fig. 15 compares the $u_F - F$ registered experimentally and obtained numerically in the strengthened prototypes, where the maximum deviation on the maximum load was smaller than 9%. This deviation in the prototypes strengthened with CFRP bars of inclined extremity at 15° (series 15) was less than 5% in all cases (C25A-15–1 ≈ 4%, C25A-15–2 ≈ 2%, C35A-15–1 ≈ 2%, C35A-15–2 ≈ 5%, C35B-15–1 ≈ 2%), while in the prototypes strengthened with CFRP bars of inclined extremity at 30° (series 30) was less than 10% (C25A-30–1 ≈ 2%, C25A-30–2 ≈ 5%, C35A-30–1 ≈ 8%, C35A-30–2 ≈ 9%, C35B-30–1 ≈ 8%, C35B-30–2 ≈ 1%). The higher deviation on the series with CFRP bars of inclined extremity at 30° is justified by the premature and progressive nature of the tensile rupture of these bars in the transition zone. The smaller internal angle of this zone regarding the series with CFRP bars of inclined extremity at 15° introduces higher local bending moments and shear forces, as demonstrated in a model dedicated to simulating these local effects [16].

Consequently, for modelling with higher accuracy the tensile behaviour of these CFRP bars, a bilinear diagram may also be used in conjunction with the proposed approach, such as the one represented in Fig. 16a. By using this relationship on the simulation of series C25A-30, a much better predictive performance in terms of the maximum load was obtained, as shown in Fig. 16b (the maximum deviation on the maximum load is now 0.8%). However, it is considered that the numerical approximation assuming the perfect bond of the CFRP already yields sufficiently good results.

4. Conclusions

Based on the relevant obtained results presented in this paper, the following conclusions can be pointed out:

- Although the CFRP bars have not yet the aimed tensile strength, they were able to increase significantly the load-carrying capacity for SLS condition ($P_{l/250}$, load at deflection $l/250$, where $l = 1000$ mm) and at failure (P_{max}). The CFRP bars bent at 15° produced an average increase of 90% for the $\overline{P}_{l/250}$ and 99% for the $\overline{P}_{max}$ (the overbar indicates the average of the tested prototypes), while the CFRP bars bent at 30° provided an average increase of 78% for the $\overline{P}_{l/250}$ and 67% for the $\overline{P}_{max}$. Therefore, $P_{l/250}$ and P_{max} tend to decrease as larger is the inclination of the bent part of the CFRP bar. This is caused by the gradient of bending moments and shear forces occurring in the

transition zone which is as larger as smaller is the radius of this zone, by anticipating the tensile rupture of this zone.

- By using the *fib* bulletin 90 formulations, the maximum load-carrying capacity of the tested strengthened balcony prototypes ($P_{R,Ana}^{Str}$) was estimated and compared to the one registered experimentally $P_{R,Exp}^{Str}$. An average ratio $P_{R,Exp}^{Str}/P_{R,Ana}^{Str}$ of 0.95 (standard deviation of 0.08) was obtained, which validates the use of this existing analytical approach for the design of strengthened balconies despite using a non-standard CFRP bar.
- The developed design-oriented numerical approach was capable of predicting with high accuracy the force–deflection obtained experimentally. The maximum deviation was less than 2% and 9% in terms of load at yield initiation and maximum load, respectively.

CRediT authorship contribution statement

J.A.O. Barros: Conceptualization, Methodology, Supervision, Software, Formal analysis, Writing – original draft. **Fábio P. Figueiredo:** Methodology, Software, Formal analysis, Writing – review & editing, Visualization. **Inês G. Costa:** Investigation, Writing – review & editing, Visualization. **Filipe Dourado:** Resources.

Declaration of Competing Interest

The authors declare that they have no known competing financial interests or personal relationships that could have appeared to influence the work reported in this paper.

Acknowledgements

References

[1] De Lorenzis L. Strengthening of RC structures with near surface mounted FRP rods. PhD thesis. Italy: Department of Innovation Engineering, University of Lecce; 2002.

[2] Teng JG, De Lorenzis L, Wang B, Li R, Wong TN, Lam L. Debonding failures of RC beams strengthened with near surface mounted CFRP strips. ASCE J Compos Constr, 10(2), 92-105.

[3] Barros JAO, Fortes AS. Flexural strengthening of concrete beams with CFRP laminates bonded into slits. J Cem Concr Compos, 27(4), 471-480.

[4] Costa IG, Barros JAO. Flexural and shear strengthening with composite materials – the influence of cutting steel stirrups to install CFRP strips. J Cem Concr Compos 2010;32:544–53.

[5] Dias SJE, Silva JRM, Barros JAO. Flexural and shear strengthening of reinforced concrete beams with a hybrid CFRP solution. Compos Struct J 2021;256:113004. https://doi.org/10.1016/j.compstruct.2020.113004.

[6] Salib MN. Flexural behavior of RC T- section beams strengthened with different configurations of CFRP laminates. Int J Curr Eng Technol 2012;2(4):418–26.

[7] Kim YJ, Bhiri M. Grid U-wrap anchorage for reinforced concrete beams strengthened with carbon fiber-reinforced polymer sheets. ACI Struct J January 2020;117(1):3–16.

[8] Bisby L, Williams VRK, Kodur VRK, Green MF, Chowdhury E. "Fire Performance of FRP Systems for Infrastructure: A State-of-the-Art Report, Institute for Research in Construction, RR-179. Kingston and National Research Council, Ottawa: Queen's University; March 2005.

[9] Firmo JP, Correia JR, Bisby LA. Fire behaviour of FRP-strengthened reinforced concrete structural elements: A state-of-the-art review. Compos B Eng 2015;80: 198–216.

[10] Barros JAO, Rezazadeh M, Laranjeira JPS, Hosseini MRM, Mastali M, Ramezansefat H. Simultaneous flexural and punching strengthening of RC slabs according to a new hybrid technique using U-shape CFRP laminates. Compos Struct J January 2017;159:600–14. https://doi.org/10.1016/j.compstruct.2016.10.009.

[11] Imjai T, Garcia R, Guadagnini M, Pilakoutas K. Strength degradation in curved fiber-reinforced polymer (FRP) bars used as concrete reinforcement. Polymers. 2020;12(8):1653. https://doi.org/10.3390/polym12081653.

[12] Firmo JP, Correia JR. Fire behaviour of thermally insulated RC beams strengthened with NSM-CFRP strips: Experimental study. Compos Part B: Eng, Volume 76, 2015, Pages 112-121, ISSN 1359-8368, https://doi.org/10.1016/j.compositesb.2015.02.018.

[13] Barros JAO, Rezazadeh M, Costa IG, Baghi H, Hosseini MRM, Mastali M, Laranjeira J. Flexural and shear/punching strengthening of RC beams/slabs using hybrid NSM-ETS technique with innovative CFRP laminates. Insights and Innovations in Structural Engineering, Mechanics and Computation, Alphose Zingoni (Eds), 5-7 September 2016, Cape Town, South Africa.

[14] Chalioris CE, Kosmidou P-M-K, Papadopoulos NA. Investigation of a New Strengthening Technique for RC beams Using Carbon FRP Ropes as Transverse Reinforcements. Fibers, MDPI 2018;6:52.

[15] Kaya E, Kutan C, Sheikh S, Ilki A. Flexural retrofit of support regions of reinforced concrete beams with anchored FRP ropes using NSM and ETS methods under reversed cyclic loading. J Compos Constr 2016;16:10–20.

[16] Silva CAN, Ciambella J, Barros JAO, Costa IG. Modelling of CFRP laminates applied according to the ETS/NSM technique. 9th International Conference on Fibre-Reinforced Polymer (FRP) Composites in Civil Engineering (CICE 2018), Paris 17-19 July 2018.

[17] Matthys S, Triantafillou T, Balázs G, Barros JAO, Bilotta, A, Bournas D, et al. Externally applied FRP reinforcement for concrete structures. fib 90 Bulletin, Technical Report, Task Group 5.1, ISBN 978-2-88394-131-1, May 2019.

[18] Model Code 2010. fib Model Code for Concrete Structures 2010. International Federation for Structural Concrete (fib). Ernst & Sohn, Berlin, Germany; 2013.

[19] Silva CAN, Ciambella J, Barros JAO, Costa IG. Analytical bond model for general type of reinforcements of finite embedment length in cracked cement based materials. Int J Solids Struct 2019;167:36–47. https://doi.org/10.1016/j.ijsolstr.2019.02.018.

[20] EN 206-1. Concrete - Part 1: Specification, performance, production and conformity. European standard, CEN, 69 pp. (2000).

[21] EN,. 10002–1, "Metallic materials - Tensile testing. Part 1: Method of test (at ambient temperature)". European Standard, CEN 1990;35:pp.

[22] ISO. 527–5, "Plastics - Determination of tensile properties - Part 5: Test conditions for unidirectional fibre-reinforced plastic composites". In: International Organization for Standardization (ISO); 1997. 9 pp..

[23] Costa Inês, Barros Joaquim. Tensile creep of a structural epoxy adhesive: experimental and analytical characterization. Int J Adhes Adhes 2015;59:115–24.

[24] ISO. 527–2, "Plastics - Determination of tensile properties - Part 2: Test conditions for moulding and extrusion plastics". International Organization for Standardization; 1993.

[25] Bilotta A, Ceroni F, Barros JAO, Costa IG, Palmieri A, Szabo ZK, et al. Bond of NSM FRP strengthening concrete: round robin test initiative. J Compos Constr 2016;20: February. https://doi.org/10.1061/(ASCE)CC.1943-5614.0000579.

[26] Varma RK. Numerical models for the simulation of the cyclic behaviour of RC structures incorporating new advanced materials. PhD thesis. University of Minho; 2013.